

N 72-13835 109 25

VELOCITY DISPERSIONS IN GALAXIES: I. THE SO GALAXY NGC 7332

Donald C. Morton and Roger A. Chevalier  
Princeton University Observatory  
Received \_\_\_\_\_

NSR 31-001-901

ABSTRACT

A coude spectrum of the SO galaxy NGC 7332 with 0.9 $\text{\AA}$  resolution from 4186 to 4364 $\text{\AA}$  was obtained with the Princeton SEC vidicon television camera and the Hale telescope. Comparisons with spectra of G and K giant stars, numerically broadened for various Maxwellian velocity distributions, give a dispersion velocity in the line of sight of  $160 \pm 20 \text{ km sec}^{-1}$  with the best fit at G8III. The dispersion appears to be constant within  $\pm 35 \text{ km sec}^{-1}$  out to 1.4 kpc ( $H = 100 \text{ km sec}^{-1} \text{ mpc}^{-1}$ ). After correction for projection, the rotation curve has a slope of  $0.16 \text{ km sec}^{-1} \text{ pc}^{-1}$  at the center and a velocity of  $130 \text{ km sec}^{-1}$  at 1.4 kpc where it is still increasing. For an estimated effective radius of 3.5 kpc enclosing half the light, the virial theorem gives a mass of  $1.4 \times 10^{11} M_{\odot}$  if the mass-to-light ratio is constant throughout the galaxy. The photographic luminosity is  $8.3 \times 10^9 L_{\odot}$  so that the M/L ratio is 17.

CASE FILE  
COPY

## I. INTRODUCTION

Our knowledge of the masses of single elliptical galaxies depends mainly on measurements of the component stars. Dispersions can be derived from a few line profiles in high resolution spectra, but such spectra have been obtained for only the very brightest galaxies (Burbidge, Burbidge, and Fish 1961 a, b, c; Minkowski 1961). The Princeton SEC vidicon television camera described by Lowrance, Morton, Zucchini, Oke, and Schmidt (1972) has proven to be an ideal detector for these observations. The low background noise permits integration times of several hours with high sensitivity so that the tube can record a small wavelength band of a faint object at high dispersion. If the spectrum is not widened, the two-dimensional TV picture also can give information on rotation and the variation of the dispersion with distance from the center. King (1963) has emphasized the importance of dispersion measurements away from the center to give constraints on the dependence of the distribution function on angular momentum. A number of spectra of SO and elliptical galaxies have now been obtained with the television camera on the coudé spectrograph of the Hale 200-inch telescope. We report here the results for the first galaxy, NGC 7332.

This galaxy has been classified as E7 by van den Bergh (1960), SO<sub>2</sub> pec by Sandage (1961), and SO pec by de Vaucouleurs and de Vaucouleurs (1964). Photographs have been published by Burbidge and Burbidge (1959), Sandage (1961), and van Houten (1961). The Burbidges noted that the nuclear region is almost rectangular and van Houten distinguished between bulge and disc components. The Burbidges also pointed out that the thin extensions of the major axis beyond the nucleus are not exactly collinear and suggested there

might be tidal interaction with the Sc galaxy NGC 7339 which is only 5' away.

The velocity dispersion of the stars in the galaxy is best derived by comparison with spectra of bright stars similar to the galaxy in spectral type. If all objects are observed with the same instrument and the same slit width, no corrections are needed for the spectrograph resolution provided the galaxy lines are well resolved. Humason, Mayall, and Sandage (1956) quoted G3 as the spectral type for both NGC 7332 and M32, but Burbidge, Burbidge, and Fish used the KOIII star  $\delta$  Tau in their analysis of M32. Consequently, we obtained comparison spectra ranging from F5III to K4III.

Various techniques have been used for broadening the lines in the star spectra to match the galaxy profiles. Minkowski depended on visual comparisons of photographs of the galaxy spectrum with sets of spectra of a star or galaxy artificially smeared to represent Gaussian distributions with various dispersions. Alternatively Burbidge, Burbidge and Fish compared intensity plots of M32 with a series for  $\delta$  Tau broadened to various dispersions by numerical calculation. The digital data arising from the reduction of the TV spectra, along with a modern computer, permit further improvements in the numerical approach as outlined in § IV.

## II. OBSERVATIONS

As described by Lowrance et al (1972) the TV camera was mounted at the focus of the 36-inch Schmidt camera of the 200-inch coude spectrograph. There the dispersion in third order was  $8.74\text{\AA mm}^{-1}$  corresponding to  $0.42\text{\AA}$  per  $48\mu$  bandwidth-limited picture element on the TV cathode. An untrailed spectrum of NGC 7332 was obtained on October 8, 1970 in a five hour exposure centered on 5:30 UT. The comparison stars HD 61064 (F5III), HD 43261 (G5III), HD 51814 (G8III) and HD 49161 (K4III) were taken later that night or the following night with exposures of 25 to 65 sec. The seeing was estimated to be about 3" for the galaxy exposure and better for the stars. The width of the spectrograph slit was set at 1mm corresponding to  $1".35$  so that after a factor 10 demagnification the projected width on the cathode was  $0.87\text{\AA}$ . The measured TV camera response to the appropriate test pattern of 5 square-wave cycles per mm was about 90 percent.

The slit was oriented north-south through the nucleus at an angle of about  $25^\circ$  to the major axis, with the image rotator in the beam. The slit length included  $27"$  of the galaxy with the nucleus approximately in the center. The TV cathode covered the range  $4160$  to  $4390\text{\AA}$ , but both ends of the frame for NGC 7332 were read out after the first two hours of the exposure to check the integrated signal strength, leaving the range  $4186$  to  $4364\text{\AA}$  for the final readout. This range included almost all the lines which Burbidge, Burbidge and Fish found suitable for determining dispersion velocities, namely  $H\gamma$ ,  $\lambda 4227$  of CaI, and several lines of FeI. A Corning 5330 filter was used to eliminate second and fourth-order wavelengths.

At the end of each exposure the vidicon target was read out in analogue form to a magnetic tape which was later digitized. Figure 1 is a

picture of the spectrum of NGC 7332 made with a mechanical film scanner from the digital record after application of the calibration factors described below. The vertical scale has been magnified 4.5 times the horizontal scale. The TV lines were nearly parallel to the dispersion with a height of  $33\mu$  or  $0''.45$ ; they are divided into digital picture elements each  $28\mu$  or  $0.25\text{\AA}$  wide. The bright spot in the middle of the spectrum, just below the nucleus resulted from an accidental switching off of the power to the camera between exposure and readout, probably causing a voltage transient which made the electron scanning beam expose this part of the target.

### III. DATA REDUCTION

#### a) Noise Filter

Since the absorption features in the galaxy spectrum were rather broad, it was desirable to filter out the high frequency noise components before comparison with the stellar spectra. Noise was introduced into the TV output primarily by the quantum fluctuations in the signal, with an additional contribution from the readout amplifier at the low light levels away from the nucleus. Following the recent discussion of the processing of spectra by Brault and White (1971), we multiplied the Fourier transform of each TV line in the galaxy frame by the filter function

$$\Phi = \frac{P_s}{P_s + P_n} \quad (1)$$

where  $P_s$  and  $P_n$  are respectively the power spectra of the signal and the noise in the galaxy spectrum. We derived the total power spectrum ( $P_s + P_n$ ) for each TV line of the galaxy directly from the digitized data by a fast Fourier transform routine. We could not know  $P_s$  for the galaxy without a noise-free exposure, but an estimate of the behaviour of  $P_s$  at high fre-

quencies was obtained from the shape of the power spectrum of the well-exposed comparison star HD 43261 in which the noise component was relatively small. Since the star has many narrow lines, its  $P_s$  must be greater than that for the galaxy at high frequencies and consequently the filtering of the galaxy was less severe than if we had used the true  $P_s$  for the galaxy.

The filter function was approximated by  $\Phi = 1$  for frequencies  $\nu \leq \nu_1$ ,  $\Phi = 0$  for  $\nu \geq \nu_2$ , and linear between  $\nu_1$  and  $\nu_2$  whose values changed gradually from one TV line to the next. For example on the TV line with maximum intensity in the nucleus we chose  $\nu_1 = 0.04$  and  $\nu_2 = 0.3$  cycles per digital element, corresponding to 440 and 58 km sec<sup>-1</sup> respectively. This filter function also was applied to the comparison star after smoothing to the dispersion of 160 km sec<sup>-1</sup> derived for the galaxy in the next section. Comparison with the unfiltered star spectrum showed that the adopted dispersion velocity was not affected by the filtering.

#### b) Intensity Calibration

Since the output of the TV camera is not linear with exposure at high intensities, the tube was calibrated at 10 intensity levels including zero, at each point on the cathode by illuminating it uniformly with a constant light source and integrating for various time intervals. It was assumed that varying the exposure time was equivalent to varying the light intensity, since some preliminary experiments have shown no evidence of reciprocity failure. Smoothed calibration factors were then applied to each picture point by point. It was necessary to watch for a shift in the zero level which occurred between the observing run at Palomar and the calibration in Princeton possibly due to changes of the target bias voltage and the base level in the tape recorder.

c) S-Distortion

The S-distortion curved the spectrum relative to the TV lines. Both galaxy and star frames were corrected for this effect by a simple transformation which was derived from the deviation of the line of maximum intensity from a specific TV line at each wavelength.

d) Tube Background and Sky

For the star exposures, both the sky signal and dark current from the TV cathode were negligible, but they made important contributions to the galaxy especially in the fainter outer parts. An estimate of the tube background on the long exposure was obtained from the region of the TV frame outside the iron comparison spectrum, but no direct sky measure was available because the galaxy covered the whole length of the slit. Since the quarter moon was up during 70 percent of the five hour exposure on NGC 7332, we finally adopted a relatively large sky correction amounting to 25% of the background on the galaxy, so that after subtraction of the background, the sky was 11% of the remaining signal from the nucleus and 45% of the signal at the end of the slit. This choice for the sky seemed reasonable because the resulting equivalent widths of the absorption lines were then nearly constant across the galaxy, particularly the H $\gamma$  line which is unlikely to show any effects of variations in stellar population.

This problem of determining the sky contribution to the continuum level in the spectrum of a galaxy shows the need for a special feature in the design of spectrographs to be used with the new generation of sensitive two-dimensional electro-optical detectors. It would be very helpful if the spectrograph were to have a path by which a dispersed sample of sky light away from the galaxy could be recorded at the same time.

#### IV. VELOCITY DISPERSION, REDSHIFT, AND ROTATION

##### a) Broadening of Stellar Spectra

We have adopted the usual assumptions that all stars contributing to the observed galaxy spectrum around  $4300\text{\AA}$  have a Maxwellian velocity distribution with the same dispersion  $\sigma$  in the line of sight, and they have the same spectral shape  $I(\lambda)$ . The composite spectrum at  $\lambda_0$ , therefore, must be

$$I'(\lambda_0) = \frac{c}{\lambda_0 \sigma \sqrt{2\pi}} \int_{-\infty}^{+\infty} I(\lambda) \exp\left[-\frac{c^2(\lambda-\lambda_0)^2}{2\lambda_0^2\sigma^2}\right] d\lambda. \quad (2)$$

To simplify computation we assumed  $\lambda_0\sigma$  rather than  $\sigma$  is constant with wavelength over the narrow range from  $4186$  to  $4364\text{\AA}$  covered by the TV spectrum of the galaxy. Thus the dispersion  $\sigma$  varied inversely with  $\lambda$  along the spectrum, but the change was only  $\pm 2\%$ . With constant  $\lambda_0\sigma$  the right-hand side is a convolution integral, and application of the convolution theorem gave the broadened spectrum  $I'(\lambda)$  from the inverse Fourier transformation of the product of the Fourier transforms of the Gaussian and an observed star spectrum  $I(\lambda)$ . In this way broadened spectra were generated for the comparison stars with many values of  $\sigma$  from  $50$  to  $200 \text{ km sec}^{-1}$ .

##### b) Velocity Dispersion

Since the seeing was about  $3''$ , averages over 7 TV lines of the galaxy spectrum were plotted for comparison with the broadened stellar spectra. In Figure 2, the average containing the brightest part of the nucleus is shown beside the G8III star with  $\sigma = 160 \text{ km sec}^{-1}$ . The region around  $\lambda 4272$  of FeI has an anomalously high intensity in the galaxy due to the nearby read-out error on the TV frame. The differential redshift in the galaxy lines causes slight deviations from the wavelengths of the star lines at each end



of the spectrum. Figures 3 and 4 also show the nucleus and the G8III star, but with  $\sigma = 140$  and  $180 \text{ km sec}^{-1}$ . At the lower dispersion velocity the stellar lines are deeper than those in the galaxy, while for the higher value,  $\lambda 4227$  of CaI is shallower in the star. Therefore we conclude that the dispersion in the center of NGC 7332 is  $160 \text{ km sec}^{-1}$ , with an uncertainty of about  $20 \text{ km sec}^{-1}$ . In our visual fitting procedure, no attempt was made to force agreement of the continuum levels over a wide wavelength range so that any difference between the energy distributions of the stars and galaxy would not influence the derived velocity.

In Figures 5 and 6 the nucleus is compared with the best fits for the G5III star at  $\sigma = 160 \text{ km sec}^{-1}$ , and K4III at  $150 \text{ km sec}^{-1}$ . The CaI line is too weak in the broadened G5III star while both CaI and FeI are too strong in the K4III star showing that these types are definitely different from the spectral class of the galaxy, which is best represented by a G8II star in our spectral region.

At  $10''$  from the center of the galaxy the decreased signal-to-noise ratio and uncertainties in the sky contribution made estimates of the dispersion much more difficult. However, it appeared to have approximately the nuclear value of  $160 \text{ km sec}^{-1}$  with the uncertainty increased to  $35 \text{ km sec}^{-1}$ . It is unlikely these numbers would change if a different sky correction had been used in § III d.

#### c) Redshift

Measurement of the centers of the lines  $\lambda 4226.7$  of CaI, and  $\lambda 4271.7$  and  $4325.7$  of FeI gave a radial velocity of  $1170 \pm 60 \text{ km sec}^{-1}$  after correction for the earth's orbital motion. This value is consistent with  $1204 \pm 50 \text{ km sec}^{-1}$  quoted by Humason, Mayall, and Sandage (1950). We have

adopted a recession velocity of  $1464 \text{ km sec}^{-1}$  derived by correcting the latter figure for the solar motion in the local group. With a Hubble constant of  $100 \text{ km sec}^{-1} \text{ mpc}^{-1}$ , the distance is 14.6 mpc.

d) Rotation

Rotational velocities were obtained at various projected distances up to  $10''$  from the center by measuring the wavelength shifts necessary to superpose plots of the nuclear region on the spectra of the outer parts. The observed rotation curve is shown in Figure 7 where the vertical bars indicate subjective estimates of the errors. The velocity changes rapidly in the central region and appears to level off farther out, though the maximum probably lies beyond the width of our spectrum. The measured radii and velocities require correction for both the inclination of the galaxy from the plane of the sky and the  $25^\circ$  deviation of the slit from the major axis. We have adopted an inclination of  $76^\circ$  from the ratio of the axes  $b/a = 0.24$  of the outermost isophote given by van Houten (1961), since he indicates the light at large distances from the center must come entirely from the disc. If we assume a simple disc model for the whole galaxy, with the surfaces of constant velocity on cylinders, equation (1) of Rubin and Ford (1970) shows that an apparent distance of  $10''$  or 710 pc along the slit is really  $2.0 \times 710 = 1420$  pc along a radius of the galaxy and the true rotational velocity at the end of this radius is  $2.2 \times 60 = 130 \text{ km sec}^{-1}$ . The true slope of the velocity curve at the center is  $0.16 \text{ km sec}^{-1} \text{ pc}^{-1}$ .

V. MASS AND LUMINOSITY OF NGC 7332

Since our velocity measures are limited to the central part of the galaxy, this is the region for which we would have the most confidence in

any derived properties such as the mass-to-light ratio. However, it is interesting to try to calculate the total mass of the galaxy under the simplifying assumptions that the observed dispersion velocity is representative of the whole galaxy and  $M/L$  is constant over the galaxy.

a) General Theory

If we assume a galaxy is in a stationary state we can estimate its mass from the relation between the kinetic energy  $T$  and potential energy  $\Omega$  given by the virial theorem,

$$2T + \Omega = 0 \quad (3)$$

Both random motions and rotation contribute to  $T$ , but for the present we shall assume the rotation is small so that

$$T = \frac{1}{2}M\langle v^2 \rangle \quad (4)$$

where  $M$  is the total mass of the galaxy and  $\langle v^2 \rangle$  is the mean square velocity averaged over all directions, and assumed to be the same for all stars.

In order to relate  $\langle v^2 \rangle$  to the observed dispersion  $\sigma$  in the line of sight, we must make an additional assumption regarding the distribution of orbital eccentricities. For pure radial motions  $\langle v^2 \rangle = \sigma^2$  at the center and decreases rapidly towards the outer regions. On the other hand, for isotropic motions  $\langle v^2 \rangle = 3\sigma^2$ . Since atmospheric seeing usually will blend the nucleus with some of the outer parts Poveda, Iturriaga, and Orozco (1960) have suggested that some combination may be more appropriate such as  $\langle v^2 \rangle = \frac{3}{2}\sigma^2$ . In another investigation for a spherical system, Poveda, Cruz, and Batiz (1960) found that 17% radial orbits plus 83% circular orbits would give constant observed dispersion across the galaxy and then  $\langle v^2 \rangle = 2\sigma^2$ . Our measurements of NGC 7332 seem to indicate constant  $\sigma$  so that we might

prefer the last relation. However, we have adopted

$$\langle v^2 \rangle = 3\sigma^2 \quad (5)$$

as did Burbidge, Burbidge, and Fish (1961) and Fish (1964) because they believed some consideration must be given to both isotropic motions outside the nucleus and the neglected rotational motions which also contribute to the total kinetic energy.

In this derivation of the mass of a galaxy it is important to remember that the brighter, more massive stars may contribute most of the light used to obtain the observed dispersion velocity, while a significant fraction of the mass could be contained in fainter low-mass stars which need not have the same  $\langle v^2 \rangle$ .

If we assume the ratio of mass to luminosity is constant across a galaxy, the distribution of light gives the total potential energy

$$\Omega = G \int_0^R \frac{M_r dM}{r} , \quad (6)$$

where  $M_r$  is the mass inside radius  $r$ . The easiest method for calculating  $\Omega$  follows the principles described by Poveda (1958) who integrated de Vaucouleur's (1953) standard luminosity distribution for elliptical galaxies. If we approximate the surface brightness in magnitudes at distance  $r$  from the center by

$$m(r) = m(0) + Ar^{\frac{1}{4}} \quad (7)$$

we can determine an effective radius  $R_{\frac{1}{2}}$  of a circle which encloses half the light by drawing a straight line through a plot of observed magnitudes versus  $r^{\frac{1}{4}}$  along the minor axis and noting where they fall by 8.33 mag from the extrapolated line at  $r = 0$ . Poveda showed that  $\Omega = -0.322GM^2/R_{\frac{1}{2}}$  in cgs units for spherical galaxies and Fish (1964) added two approximate corrections

for ellipticals. Since  $R_{\frac{1}{2}}$  is normally determined from measures along the minor axis, the expression for  $\Omega$  must be multiplied by  $(b/a)^{2/3}$  where  $b/a$  is the apparent ratio of minor and major axes. Also the coefficient should be increased to 0.34 to correct for the projection effect which makes the apparent ratio of axes in ellipticals average 16% less than the true ratio of equatorial and polar axes. Thus,

$$\Omega = -0.34 \frac{GM^2}{R_{\frac{1}{2}}} \left(\frac{b}{a}\right)^{2/3} \quad (8)$$

where the constant is appropriate for cgs units. Our equation (8) corrects a slight error in Fish's calculation of the coefficient and his apparently mistaken inversion of the ratio  $b/a$ . In practice the effective radius is always described by an angle  $\beta_{\frac{1}{2}}$  leaving  $R_{\frac{1}{2}}$  to be calculated from a distance estimate which is usually obtained from the recession velocity  $V$  and the Hubble constant  $H$ .

We can combine equations (3), (4), (5) and (8) to give

$$\frac{M}{M_{\odot}} = 100 \sigma^2 \beta_{\frac{1}{2}} V \left(\frac{100}{H}\right) \left(\frac{a}{b}\right)^{2/3} \quad (9)$$

where  $\sigma$  and  $V$  are now in  $\text{km sec}^{-1}$ ,  $H$  is in  $\text{km sec}^{-1} \text{ mpc}^{-1}$ , and  $\beta_{\frac{1}{2}}$  is in arc sec.

#### b) Application to NGC 7332

We estimated  $\beta_{\frac{1}{2}}$  by matching van Houten's (1961) photometry along the minor axis to de Vaucouleur's law. A good fit was not possible because the light of NGC 7332 diminished faster with increasing radius than expected from the law, but the effective radius for half the light probably lies between 5" and 25". We have given most weight to the photometry of the

brighter parts of the galaxy and adopted  $\beta_{\frac{1}{2}} = 20''$ . Van Houten's data also show that the axial ratio ranges from 0.50 near the center, to 0.24 at the outermost isophate. We have used  $b/a = 0.40$  in equation 9. At the distance of 14.6 mpc, the radius  $R_{\frac{1}{2}} = 3.5$  kpc, after correcting for projection. At a true radius of 1.4 kpc or  $0.4 R_{\frac{1}{2}}$  we found  $V_{\text{rot}} = 130 \text{ km sec}^{-1}$ . According to Table 2 of Poveda, Iturriaga, and Orozco (1960), 80 percent of the mass of a spherical galaxy lies outside this radius. If the average rotational velocity of all this mass is  $130 \text{ km sec}^{-1}$ , the rotational contribution to the kinetic energy is about 50 percent of  $\frac{1}{2} M \sigma^2$  so that our use of  $\langle v^2 \rangle = 3\sigma^2$  instead of  $2\sigma^2$  probably accounts for the rotation more than adequately. Therefore we find the mass is

$$\frac{M}{M_{\odot}} = 1.4 \times 10^{11} \left( \frac{100}{H} \right). \quad (10)$$

#### b) Photographic Luminosity

We have calculated the luminosity of NGC 7332 over the photographic band from the integrated  $m_{\text{pg}} = 11.9$  quoted by Van Houten and a galactic extinction of  $0.25 \text{ cscb} = 0.5 \text{ mag}$ . The distance derived from the Hubble law gave an absolute magnitude  $M_{\text{pg}} = -19.4 - 5 \log (100/H)$ . Stebbins and Kron (1957) obtained  $M_{\text{pg}} = 5.37$  for the sun so that the ratio of photographic luminosities must be  $L/L_{\odot} = 8.3 \times 10^9 (100/H)^2$ . The ratio of mass to luminosity for NGC 7332 is then  $\frac{M}{L} = 17 \frac{M_{\odot}}{L_{\odot}} \left( \frac{H}{100} \right)$ .

### VI. DISCUSSION

Velocity dispersions have been determined by the methods mentioned in §I for 13 E and SO galaxies. According to the summary by Minkowski (1961) the values range from  $100 \text{ km sec}^{-1}$  for the E2 dwarf NGC 221 (M32) to  $480 \text{ km}$

$\text{sec}^{-1}$  for the EOp giant NGC 4486 (M87). Four SO galaxies lie between 195 and  $270 \text{ km sec}^{-1}$ . Thus our value of  $160 \text{ km sec}^{-1}$  for NGC 7332 is consistent with previous SO measures, although it now has the second lowest known dispersion velocity.

Rotation has been found in four other spherical galaxies. Our central slope of  $0.16 \text{ km sec}^{-1} \text{ pc}^{-1}$  is comparable with the values of 0.22 and  $0.50 \text{ km sec}^{-1} \text{ pc}^{-1}$  reported by King and Minkowski (1966) for the E 5 galaxies NGC 4621 and 4697 respectively. In contrast, Walker (1962) measured  $7.8 \text{ km sec}^{-1} \text{ pc}^{-1}$  in M32 and Minkowski's (1966) measures near the center of the E7-SO galaxy NGC 3115 indicated a slope of  $2 \text{ km sec}^{-1} \text{ pc}^{-1}$ .

Genkin and Genkina (1969) have listed masses for eight elliptical galaxies derived from velocity dispersions by the principles described in this paper. For the more elongated types their values must be increased by factors up to two because they followed Fish and incorrectly used  $(b/a)^{2/3}$  in equation 9. Six of the galaxies lie in the range of approximately 1 to  $2 \times 10^{12} M_{\odot}$  while M32 is about  $3 \times 10^9 M_{\odot}$ . Only NGC 3379 with  $M \sim 1 \times 10^{11} M_{\odot}$  is comparable to the  $1.4 \times 10^{11} M_{\odot}$  we found for NGC 7332. Our M/L ratio of 17 is within a factor two of the ratios for M32, NGC 3379, and NGC 4472, but smaller than the values ranging from 50 to 120 found for five of the six massive ellipticals.

Masses and M/L ratios for double galaxies have been derived by Page (1962, 1966) on the assumption of circular orbits. For 19 E and 8 SO galaxies with measurements of the highest weight, he obtained an average mass of  $(5.9 \pm 1.5) \times 10^{11} M_{\odot}$  and an average M/L ratio of  $90 \pm 37$ . This ratio is higher than we found for NGC 7332 but consistent with the M/L values derived from the widths of the absorption lines in five massive ellipticals. Further analysis of the data on double galaxies is in order following the approach of

Wolf and Bahcall (1972) to better define the limits of the uncertainty in the average mass. At the same time, since either of the assumptions of constant velocity dispersion or constant  $M/L$  usually used in the application of the virial theorem to a single galaxy could be seriously in error, it is desirable to obtain masses for some pairs of galaxies by both methods. Thus a determination of the radial velocity of NGC 7339, the apparent companion of NGC 7332, could be very useful. Our measurement of the dispersion velocity in NGC 7332 really gives information about only the central stars whose light contributes to the observed spectrum. If the mass falls off less rapidly with radius than the light, as suggested by data on the Milky Way and M31, much of the mass of NGC 7332 could lie in the faint outer parts and then the average  $M/L$  would be considerably larger.

We wish to thank Dr. J.B. Oke of the Hale Observatories for making part of his observing time on the 200-inch telescope available to us and for suggesting the problem of velocity dispersions in galaxies. John Lowrance, Paul Zucchini, and John Opperman of the Princeton University Observatory assisted in the installation and operation of the camera at Palomar. Dr. Philip Crane of the Princeton Physics Department provided the intensity calibration and Dr. Edward Jenkins of the Princeton Observatory contributed helpful advice on the numerical noise filter and convolution integrals. The development and use of the SEC vidicon was supported by the National Aeronautics and Space Administration under contract NSR-31-001-127 to Princeton University. The analysis of the data was supported through NASA contract NSr-31-001-901 (D.C.M.) and a National Science Foundation graduate fellowship (R.A.C.).



REFERENCES

- Bergh, S. van den, 1960, Publ. of D. Dunlap Obs. II, Nr. 6.
- Brault, J.W. and White, O.R. 1971, Astron. and Ap., 13, 169.
- Burbidge, E.M., Burbidge, G.R., and Fish, R.A. 1961a, Ap. J. 133, 393.  
\_\_\_\_\_. 1961b, Ap. J. 133, 1092.  
\_\_\_\_\_. 1961c, Ap. J. 134, 251.
- Burbidge, E.M., and Burbidge, G.R. 1959, Ap. J., 130, 20.
- Fish, R.A. 1964, Ap. J. 139, 284.
- Genkin, I.L., and Genkina, L.M. 1969, Astron. Zhurnal, 46, 1128.
- Houten, C.J. van 1961, B.A.N., 16, 1.
- Humason, M.L., Mayall, N.U., and Sandage, A.R. 1956, A.J., 61, 97.
- King, I.R. 1963, Ann. Rev. Astron. and Ap., 1, 179.
- King, I.R. and Minkowski, R. 1966, Ap. J., 143, 1002.
- Lowrance, J.L., Morton, D.C., Zucchini, P., Oke, J.B., and Schmidt, M. 1972,  
Ap. J., 171, 000.
- Minkowski, R. 1960, Ann d'Ap. 23, 385.
- Minkowski, R. 1961, Problems of Extragalactic Research, ed. G.C. McVittie  
(New York: Macmillan Co.), p. 112.
- Page, T.L. 1962, Ap. J., 136, 685.  
\_\_\_\_\_. 1966, Proc. Fifth Berkeley Symp. Math. Stat. and Prob., 3, 31.
- Poveda, A. 1958, Bol. Obs. Tonantzintla y Tacubaya, 17, 3.
- Poveda, A., Cruz, C., and Batiz, G. 1960, A.J. 65, 497.
- Poveda, A., Iturriaga, R., and Orozco, I. 1960, Bol. Obs. Tonantzintla y  
Tacubaya; 20, 3.

Rubin, V.C., and Ford, W.K. 1970, Ap. J., 159, 379.

Sandage, A.R. 1961, The Hubble Atlas of Galaxies, Carnegie Institution of  
Washington Publ. No. 618.

Stebbins, J. and Kron, G.E. 1957, Ap. J., 126, 266.

Vaucouleurs, G. de. 1959, Handbuch der Physik, 53, 311. (Berlin: Springer)

Vaucouleurs, G. de and Vaucouleurs, A. de 1964, Reference Catalogue of Bright  
Galaxies (Austin: University of Texas Press).

Vaucouleurs, G. de 1953, M.N.R.A.S. 113, 134.

Walker, M.F. 1962, Ap. J. 136, 695.

Wolf, R.A., and Bahcall, J.N. 1972, Ap.J., (in press).

FIGURE CAPTIONS

Figure 1

The spectrum of NGC 7332, reproduced from the digitized data obtained on the integrating SEC vidicon television camera. The spectrum covers the range from 4186 to 4364Å with wavelengths increasing to the right. The horizontal TV scan lines are divided into digital picture elements. The vertical scale has been magnified 4.5 times relative to the horizontal scale. The comparison spectrum is an iron arc and the emission line crossing the spectrum at the far right is  $\lambda$  4358.3 of HgI in the night sky. The bright spot just under the nucleus was accidentally added to the TV target between exposure and readout.

Figure 2

The adopted fit of the galaxy spectrum (solid line) with the G8III star (dotted line) broadened to  $\sigma = 160 \text{ km sec}^{-1}$ . The peak in the middle of the galaxy spectrum is a spurious intensity increase due to an electronic failure just prior to readout. The continuum level of the G8III star fell below the galaxy at the shortest wavelengths. The widths of the weaker lines in the iron arc show that the resolution is about  $0.9\text{\AA}$ .

Figure 3

Comparison of the galaxy (solid line) with the G8III star (dotted line) broadened to  $\sigma = 140 \text{ km sec}^{-1}$ , a lower limit on the acceptable dispersion velocity.

Figure 4

Comparison of the galaxy (solid line) with the G8III (dotted line) broadened to  $\sigma = 180 \text{ km sec}^{-1}$ , an upper limit on the acceptable dispersion velocity.

Figure 5

Comparison of the galaxy (solid line) with the G5III star (dotted line) broadened to  $\sigma = 160 \text{ km sec}^{-1}$ , the best fit for this spectral type. Note that this star better reproduces the continuum level of the galaxy, but the line profiles do not fit as well as with the G8III star.

Figure 6

Comparison of the galaxy (solid line) with the K4III/ (dotted line) star broadened to  $\sigma = 150 \text{ km sec}^{-1}$ , the best fit for this spectral type. Here neither the line profiles nor the slope of the continuum resemble the galaxy very well.

Figure 7

The observed rotation curve for NGC 7332 before correction for the  $25^\circ$  deviation of the slit from the major axis. The vertical bars are subjective estimates of the errors.

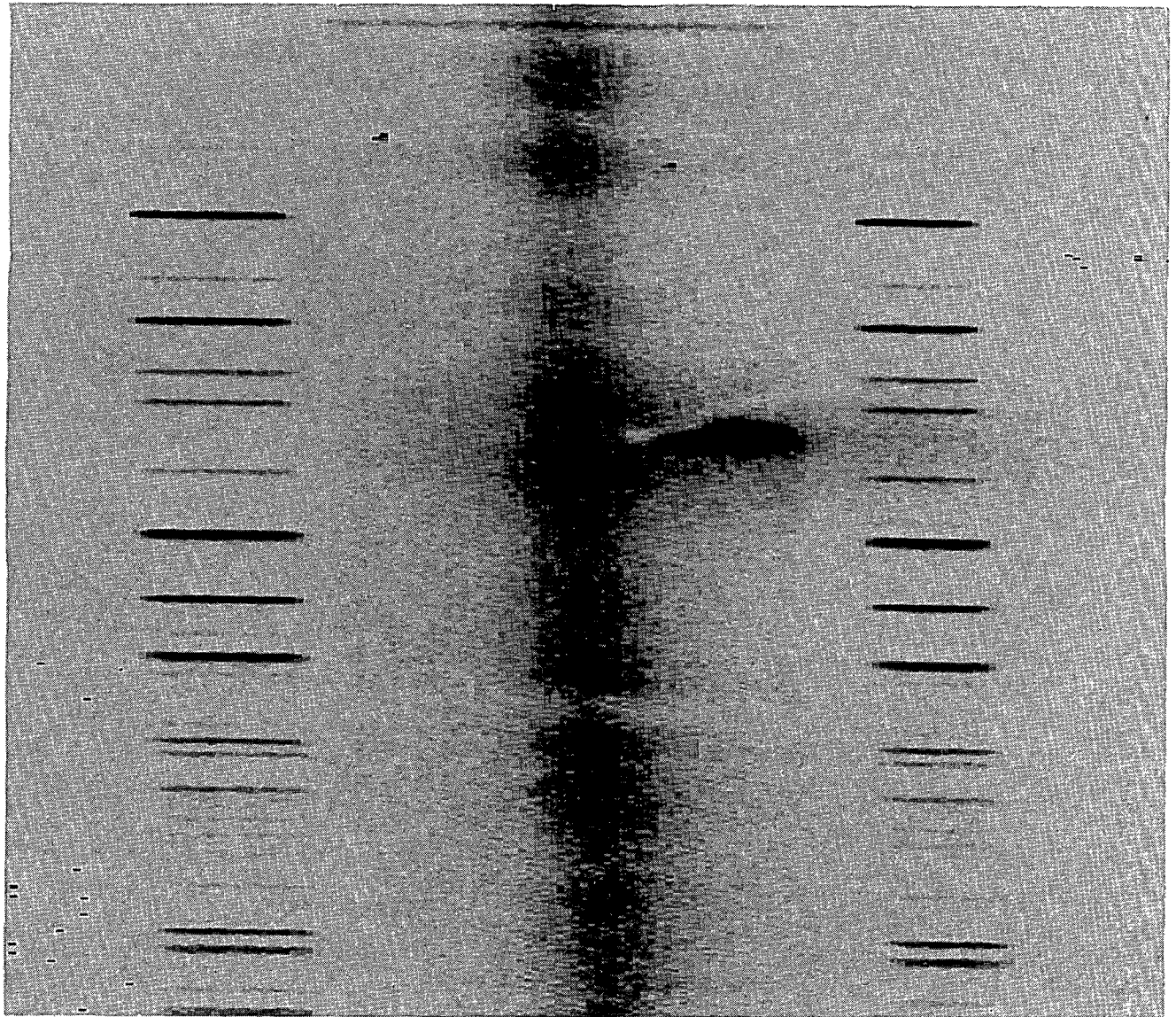


FIG. 2.

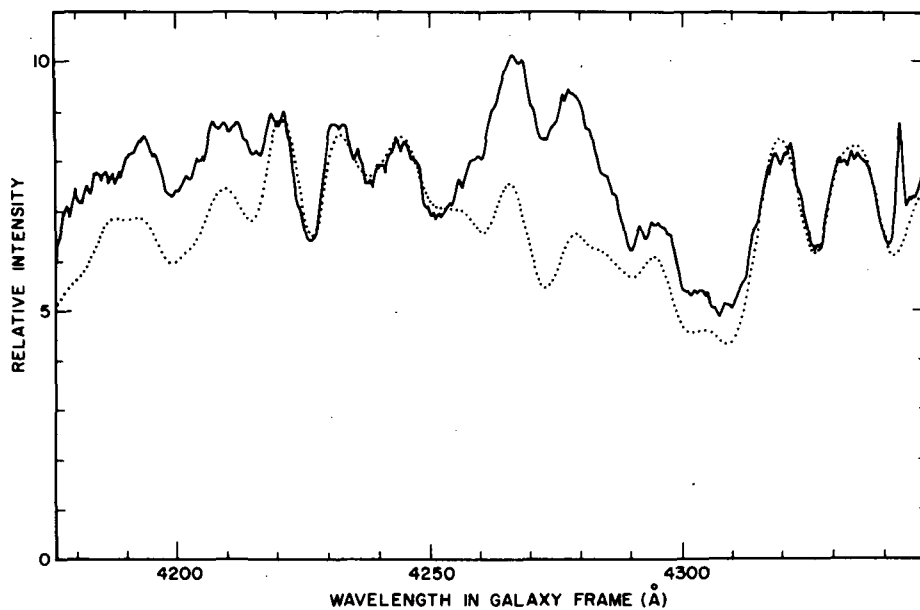


FIG. 3.

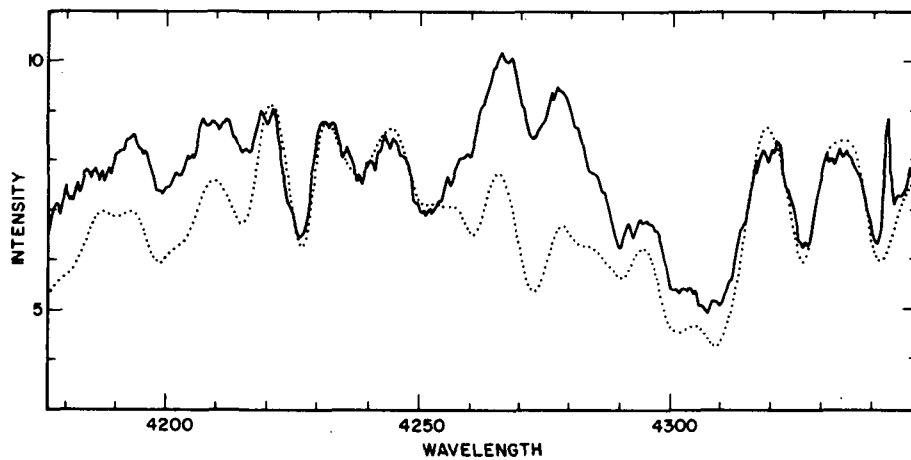


FIG. 4.

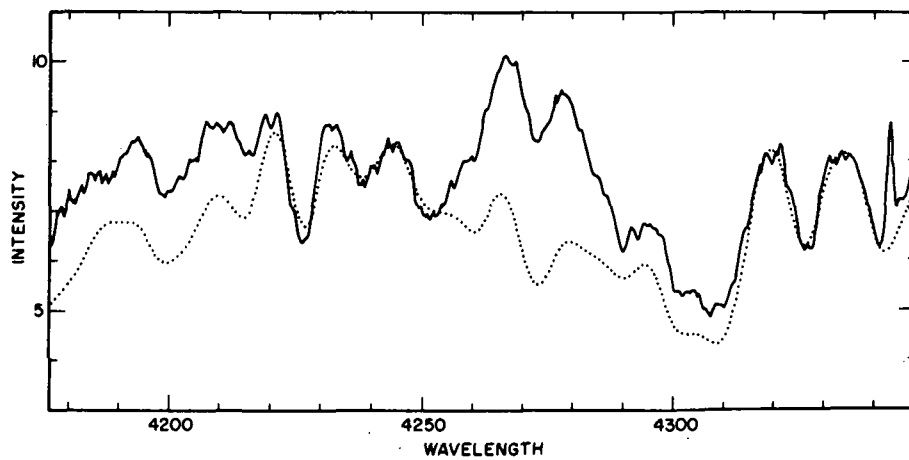


FIG. 5.

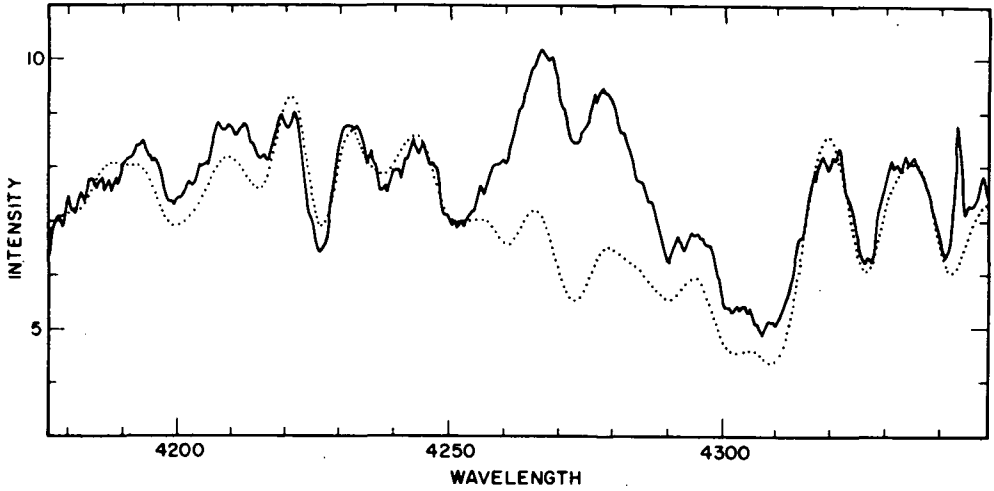


FIG. 6.

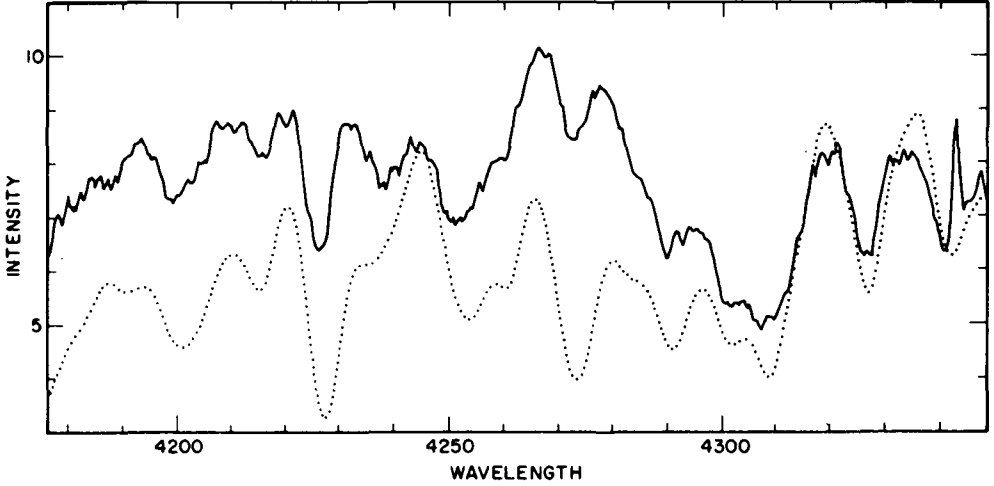


FIG. 7.

